J Neurophysiol 117: 786–795, 2017.
First published November 30, 2016; doi:10.1152/jn.00650.2016.

RESEARCH ARTICLE | *Sensory Processing*

Automated classification of pain perception using high-density electroencephalography data

Gaurav Misra, Wei-en Wang, Derek B. Archer, Arnab Roy, and Stephen A. Coombes
Laboratory for Rehabilitation Neuroscience, Department of Applied Physiology and Kinesiology, University of Florida, Gainesville, Florida

Submitted 15 August 2016; accepted in final form 28 November 2016

Misra G, Wang WE, Archer DB, Roy A, Coombes SA. Automated classification of pain perception using high-density electroencephalography data. *J Neurophysiol* 117: 786–795, 2017. First published November 30, 2016; doi:10.1152/jn.00650.2016.—The translation of brief, millisecond-long pain-eliciting stimuli to the subjective perception of pain is associated with changes in theta, alpha, beta, and gamma oscillations over sensorimotor cortex. However, when a pain-eliciting stimulus continues for minutes, regions beyond the sensorimotor cortex, such as the prefrontal cortex, are also engaged. Abnormalities in prefrontal cortex have been associated with chronic pain states, but conventional, millisecond-long EEG paradigms do not engage prefrontal regions. In the current study, we collected high-density EEG data during an experimental paradigm in which subjects experienced a 4-s, low- or high-intensity pain-eliciting stimulus. EEG data were analyzed using independent component analyses, EEG source localization analyses, and measure projection analyses. We report three novel findings. First, an increase in pain perception was associated with an increase in gamma and theta power in a cortical region that included medial prefrontal cortex. Second, a decrease in lower beta power was associated with an increase in pain perception in a cortical region that included the contralateral sensorimotor cortex. Third, we used machine learning for automated classification of EEG data into low- and high-pain classes. Theta and gamma power in the medial prefrontal region and lower beta power in the contralateral sensorimotor region served as features for classification. We found a leave-one-out cross-validation accuracy of 89.58%. The development of biological markers for pain states continues to gain traction in the literature, and our findings provide new information that advances this body of work.

NEW & NOTEWORTHY The development of a biological marker for pain continues to gain traction in literature. Our findings show that high- and low-pain perception in human subjects can be classified with 89% accuracy using high-density EEG data from prefrontal cortex and contralateral sensorimotor cortex. Our approach represents a novel neurophysiological paradigm that advances the literature on biological markers for pain.

pain; classification; medial prefrontal cortex; gamma; EEG

PAIN IS DEFINED BY THE International Association for the Study of Pain (2016) as an unpleasant sensory and emotional experience. Advances in brain imaging technologies have led to models that use neurological signals to classify pain states (Schulz et al. 2012; Wager et al. 2013). Models based on EEG data come from experiments that measure signals from electrodes over sensorimotor cortex following short-duration sensory stimuli (~5 ms laser stimulus) (Gross et al. 2007; Ploner et al. 2006; Schulz et al. 2012). In contrast, models based on functional MRI (fMRI) data come from paradigms in which the sensory input spans multiple seconds (Coombes and Misra 2016; Misra and Coombes 2015; Oshiro et al. 2009; Wager et al. 2013). fMRI models are also based on whole-brain analyses and identify regions beyond sensorimotor cortex that play a role in the sensory, cognitive, and emotional components of pain, such as medial prefrontal cortex, cingulate cortex, basal ganglia, and insula (Apkarian et al. 2009; Borsook et al. 2007; Coghill et al. 1999; Oshiro et al. 2009). The goal in the current study is to combine high-density EEG with a paradigm in which low- and high-intensity pain-eliciting stimuli span multiple seconds. We also implement EEG analysis in source space to determine whether oscillations in regions beyond the sensorimotor cortex contribute to the classification of pain perception.

Pain-related oscillations recorded over contralateral sensorimotor cortices are associated with increased theta and gamma power, 150–350 ms after laser stimuli, whereas reductions in alpha and beta power continue for up to 1,000 ms after stimulus offset (Gross et al. 2007; Ploner et al. 2006; Schulz et al. 2012). However, when sensory stimuli are longer in duration and span 10 min rather than ~5 ms, pain perception correlates positively with gamma power in medial prefrontal cortex (Schulz et al. 2015). Oscillations over sensorimotor cortex have therefore been associated with sensory processes, whereas longer-duration stimuli engage the medial prefrontal cortex and have been associated with the integration of sensory, cognitive, and emotional processes (Misra and Coombes 2015; Schulz et al. 2015; Shackman et al. 2011). What is not clear, however, is whether a pain-eliciting stimulus that lasts a few seconds is sufficient to elicit changes in oscillatory power in medial prefrontal cortex and whether oscillatory power in this region can be used to classify EEG signals according to pain perception.

Experimental pain paradigms that assess medial prefrontal cortex function are important because abnormalities in medial prefrontal cortex have been found across different chronic pain states (Apkarian et al. 2009; Baliki et al. 2012). In the current experiment, we measure high-density EEG during a 4-s con-

Address for reprint requests and other correspondence: S. A. Coombes, Laboratory for Rehabilitation Neuroscience, Dept. of Applied Physiology and Kinesiology, Univ. of Florida, P.O. Box 118206, Gainesville, FL 32611 (e-mail: scoombes@ufl.edu).

tinuous thermal stimulus. We analyze the EEG data using a measure projection analysis (MPA), which is a recently developed statistical method for characterizing the spatial localization and consistency of EEG measures in source space rather than electrode space (Bigdely-Shamlo et al. 2013). It allows the use of EEG as a 3-dimensional (3D) cortical imaging modality. Each subject experienced low- and high-pain-eliciting stimuli. We test the hypothesis that compared with the low-pain condition, the high-pain condition would lead to a sustained increase in gamma power in the medial prefrontal cortex and a sustained decrease in beta power in sensorimotor areas. We also use a support vector machine (SVM) classifier to test whether EEG measures in source space can be used to classify low- and high-pain states.

METHODS

Participants. Thirty right-handed adults (20 ± 2 yr; 16 women), with normal or corrected-to-normal vision, were recruited for this study. Participants were asked to refrain from consuming caffeine and using any hair products on the day of testing. Before experimental testing, participants provided informed consent. This experimental study was approved by the University of Florida Institutional Review Board. Since depression and anxiety have been shown to influence how experimental pain is experienced (Rhudy and Meagher 2000; Weiss et al. 2011), all participants completed the state segment of the State-Trait Anxiety Inventory (Spielberger 1983), Beck Depression Inventory (Beck and Steer 1987), and Tampa Scale of Kinesiophobia (Kori et al. 1990). All scores were within the normal range of responses given by adult participants (State-Trait Anxiety Inventory: mean = 28.69, SD = 8.14; Beck Depression Inventory: mean = 4.06, SD = 4.74; Tampa Scale of Kinesiophobia: mean = 30.9, SD = 4.8) (Beck and Steer 1987; Spielberger 1983; Thomas et al. 2008).

Thermal stimulation. Thermal stimuli were delivered to the right forearm using a 573-mm^2 contact heat-evoked potential stimulator thermode (Pathway System; Medoc Advanced Medical Systems, Durham, NC). The contact heat-evoked potential stimulator thermode was set to heat up at a rate of 70°C/s and cool down at a rate of 40°C/s. The high rates enabled reaching the requisite pain-eliciting temperatures (~45°C) from baseline (30°C) in ~0.2 s. Hence, the onset and offset of heat were precisely controlled.

Thermal stimuli were delivered to three spatially distinct sites on the right forearm of the participants, as shown in Fig. 1. The reason for choosing multiple rather than one site was to avoid sensitization and habituation, which result from stimulating the same site multiple times in a short time window.

The sites were separated by the width of the thermode, which was ~4 cm. The temperatures needed to elicit low and high pain were determined for each participant before the experiment using a calibration paradigm. During the calibration, the sites on the right forearm sequentially experienced eight pseudorandomized temperatures (41–48°C). Each trial lasted for 4 s, and the trials were separated by 10 s of rest. After each stimulation, participants used a scroll wheel to rate the pain on a visual analog scale (VAS) presented on the screen. The scale ranged from 0 to 10, with 0 being no pain and 10 being intolerable pain. The VAS was anchored with the words "no pain" and "intolerable pain." No numbers were visible to the subject. Intolerable pain was defined as the pain at which the thermode had to be removed from the forearm. For each participant, the temperature corresponding to a rating of one was used to elicit low pain, and the temperature corresponding to a rating of five was used to elicit high pain during the experiment.

Experimental design and task. The experiment was comprised of two conditions: low pain and high pain. Each participant completed 48 trials of each condition in 4 alternating blocks of low and high pain. Each block comprised of 24 trials for either low pain or high pain. Hence, the participants knew beforehand the type of trial they were about to perform. Block order was counterbalanced across subjects. Participants sat in a chair with the right arm supinated on a table in front of them. As shown in Fig. 1*A*, the three sites were outlined and numbered one through three with a skin marker. Figure 1*C* shows the timeline of events during one trial. At the start of each rest period, the index of the site to be stimulated on the upcoming trial was presented, and this was the cue for subjects to move the thermode to that site. The rest period was 10 s. Then the thermode heated up for 4 s to elicit either high pain or low pain depending on the condition. Thereafter, a VAS for rating the thermal stimulus appeared on the screen for 7 s (Fig. 1*B*). The participants used the scroll wheel held in their supinated right hand to record their pain rating for that trial. The screen then displayed the index of the next stimulation site, and the thermode was moved to that location. Rotation through three sites allowed an interstimulus period of ~1 min for each site to minimize the possibility of sensitization or habituation at any single site.

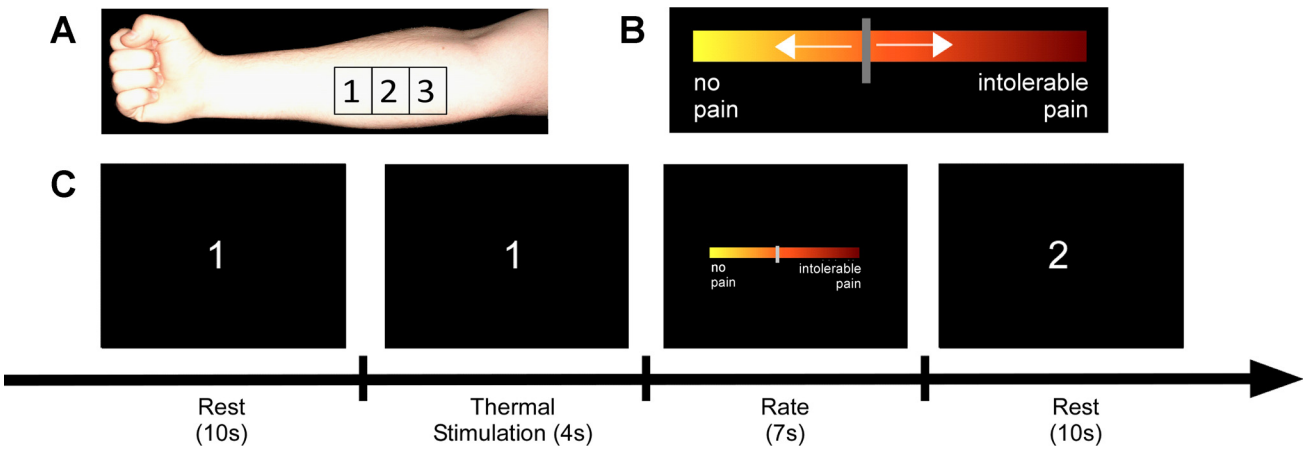

Fig. 1. Setup and trial timeline. The experiment was comprised of 2 conditions: low- and high-pain-eliciting stimuli, delivered to 3 sites on the forearm. *A*: positions of the 3 stimulation sites on the forearm of the subject are shown. The separation between the sites was ~4 cm. *B*: the visual analog scale (VAS) for rating the heat pain. Extreme *left* indicated no pain, extreme *right* indicated intolerable pain, and the *middle* indicated moderate pain. *C*: the subject's view of the screen. The trial started with a 10-s rest period, during which the index of the site to be stimulated was shown on the screen, and the thermode was placed on that site. Thereafter, the thermode was heated to a subject-specific and condition-specific temperature within 0.2 s and stayed on for 4 s, after which, the VAS appeared on the screen for 7 s, and the subject rated the pain experience. Then the rest period started again with the screen showing the index of the site to be stimulated in the next trial. A block consisted of 24 successive trials of the same condition. Two blocks of each condition were performed.

Data acquisition. The MotionMonitor system (Innovative Sports Training, Chicago, IL) was configured to record data in real time from the EEG system. A custom LabVIEW program was used to control the visual display, trigger the thermode in synchrony with the EEG recordings, and collect the pain ratings.

EEG data acquisition. EEG data were collected with the ActiveTwo system that comprised 128 Ag-AgCl active electrodes and a 256-channel AD-box (BioSemi, Amsterdam, Netherlands). The ActiveTwo system replaces the conventional ground electrode with two separate electrodes: common mode sense and driven right leg. These two electrodes form a feedback loop, which drives the average potential of the subject as close as possible to the reference voltage in the AD-box. The electrode offsets—the running averages of the voltages measured between the common mode sense and each active electrode—were measured before the start of each session and were kept below 40 μV.

The active electrodes were connected to a head cap that was in a preconfigured, 128-electrode montage covering the entire scalp. The head-cap size was selected based on the participant's head circumference (50–54, 54–58, or 58–62 cm). Standard protocols for placement of the cap were followed, such that the apex electrode, which corresponded with the Cz electrode of the international 10-20 system (Jasper 1958), lay midway between the tragi and midway between the nasion and the inion. The ActiveTwo system has an analog input and a digital output. The scaling between the digital output range (2^{23} to -2^{23}) and the analog input range (262,144 to $-262{,}144$ mV) was 32 bits/mV. EEG signals were sampled at 2,048 Hz for recording the raw data. Data were downsampled to 1,000 Hz for analysis.

EEG data preprocessing. EEG data were analyzed using the EEGLAB Toolbox (Delorme and Makeig 2004) for MATLAB (version 2014a; MathWorks, Natick, MA) and custom MATLAB scripts. EEG signals were high-pass filtered at 0.25 Hz. EEG channels were screened for large fluctuations as follows. The mean SD was calculated by averaging the SDs of all channels. Any channel with an SD $>$ 4 times the mean SD was rejected and then interpolated from the neighboring channels. The interpolation procedure weighted the remaining channels with the inverse of their respective distance from the channel to be reconstructed. On an average, two channels per trial per subject were rejected and interpolated. The EEG signals were then re-referenced to the global average of all EEG channels. Heat onset was defined as the event for aligning the EEG signal across trials. Thereafter, 5.5 s-long epochs, from 1.5 s before the event to 4 s after the event, were extracted from each trial and aligned at the event.

Independent component analysis and artifact removal. EEG data were prepared for further analysis by concatenating all epochs across all conditions within each subject. The infomax independent component analysis (ICA) algorithm (Bell and Sejnowski 1995) with the natural gradient feature (Amari et al. 1996) was used to decompose the concatenated EEG data of each subject into maximally independent components. The ICA enabled automated detection and removal of stereotyped eye, muscle, and line noise artifacts. We used the Multiple Artifact Rejection Algorithm (MARA) Toolbox for automated artifact rejection (Winkler et al. 2011) with custom modifications to optimize the algorithm for our data. MARA uses a linear, pretrained classifier that performs a binary classification (artifact or nonartifact) in a 6D feature space. However, due to task-based differences between the training dataset of MARA and our data, MARA rejected many nonartifactual components in our data. Custom modifications were therefore made to MARA to include the prior probability of a component being artifactual. The default value of prior probability was 0.5. We varied the prior probability to identify the value at which the MARA Toolbox stopped rejecting nonartifactual components in a subset of our dataset. The prior probability of a component being artifactual was identified to be 0.15, and we used this value to analyze the full dataset. After artifact rejection, a second round of ICA was run to maximize brain source-related independent components.

EEG source localization. Source localization of each independent component was performed using the DIPFIT Toolbox, which computes an equivalent current dipole model that best explains the scalp topography of each independent component. An equivalent current dipole model was fitted using a nonlinear optimization technique (Scherg 1990) and the analytical spherical head model from Brain Electrical Source Analysis (BESA; Gräfelfing, Germany), which uses four spherical surfaces (skin, skull, cerebrospinal fluid, and cortex) to model the electrical properties of the human head (Kavanagh et al. 1978). The BESA head model has a template channel location map based on the standard 10-5 system. The actual channel location map was mapped onto the BESA template channel location map, which in turn, was coregistered to the Montreal Neurological Institute (MNI) brain template. Independent components, for which 15% or more of the channel variance in the scalp map could not be accounted for by a single equivalent dipole, were removed from further analysis (Bigdely-Shamlo et al. 2013). Independent components, for which the equivalent dipoles were located outside the MNI brain (minimum distance to the MNI brain surface was larger than 1 mm), were also removed from further analysis.

EEG measures. Three measures were calculated for each independent component that was source localized within the MNI brain template: event-related spectral perturbation (ERSP), event-related potential (ERP), and intertrial coherence (ITC). Sinusoidal wavelet transform was used to convert the independent component EEG data from the time domain to the time-frequency domain to obtain the spectral estimate at each frequency and time point for each trial. The 1.5-s time window before the event served as the baseline relative to which spectral perturbations were calculated over the 4-s window after the event. Spectral estimates after the event were baseline normalized by subtracting the mean baseline log-power spectrum from each spectral estimate. The complex norms of the normalized spectral estimates were squared and averaged across trials to obtain the ERSP value at each frequency and time (Delorme and Makeig 2004). The baseline-normalized spectral estimate at each frequency and time point was length normalized by its complex norm, which is also its vector length, and averaged across trials to obtain the ITC measure, also known as the phase-locking factor (Tallon-Baudry et al. 1996). ERPs were obtained by averaging the timeline of independent components that were source localized in the spatial vicinity of each other using an MPA. We also completed the analysis without first applying the baseline-normalization procedure. Results were essentially unchanged, and so for brevity, we only report results using the baseline-normalized approach.

EEG MPA. MPA is a statistical method for characterizing the localization and consistency of EEG measures across sessions of EEG recordings (Bigdely-Shamlo et al. 2013). It allows the use of EEG as a 3D cortical imaging modality with near-centimeter-scale spatial resolution. MPA was used through the Measure Projection Toolbox of EEGLAB and included the following five steps: *1*) the locations of equivalent dipoles were overlaid on a 3D grid of voxels placed with 8 mm spacing inside the MNI brain template. *2*) EEG measures for the dipole-localized independent components were spatially smoothed using a truncated 3D spatial Gaussian kernel. The SD of the Gaussian was set to 12 mm, and its extent was truncated to 3 SD (36 mm) to prevent spurious effects from distant dipoles. *3*) A pairwise independent component similarity matrix was constructed by calculating the signed mutual information between each independent component pair measure. The similarity matrix was used to calculate convergence, which was the voxel-wise, expected value of measure similarity. Convergence was a scalar and was larger for areas in which the measures associated with local independent components were similar. A P value for the convergence value at each voxel was obtained by bootstrap statistics. False discovery rate testing was used to correct for multiple comparisons at a group-wise error rate of 0.05 (Benjamini and Hochberg 1995). A critical P value of 0.002 was obtained from false discovery rate testing, and voxels with convergence $P < 0.002$

were selected to define the "measure convergence subspace" of voxels at which the local similarity of independent component measures was statistically significant. *4*) Within the measure convergence subspace, voxel groups that sufficiently differed from each other in their measure were identified by using affinity clustering, which automatically groups voxels into clusters, referred to as domains, based on the maximum allowed correlation between cluster exemplars. Maximal exemplar-pair similarity was set to a correlation value of 0.8, which is similar to previous evidence (Ofori et al. 2015). To define anatomical regions, the toolbox incorporates the probabilistic atlas of human cortical structures provided by the Laboratory of Neuro Imaging (LONI) project (Shattuck et al. 2008). *5*) Condition difference testing was implemented, where for each identified domain and subject, statistical significance of differences between measures in the two conditions was computed by first projecting the measure associated with each condition to each voxel in the domain, producing the projected measure. Then the projected measure at a voxel was weighted by the dipole density at that voxel, summed across all domain voxels, and normalized by the total domain voxel density to obtain a weighted-mean measure across all domain voxels. Bootstrapped *t*-tests with 1,000 sample sets were applied to the collection of subject-mean projected measures in the two conditions to determine significant differences between conditions. Significant values ($P < 0.05$) for each contrast were retained, and nonsignificant values were masked with zeros (Bigdely-Shamlo et al. 2013).

Outcome measures and statistical analyses. ERSP analyses were used to assess changes in spectral power within and across conditions. ERP and ITC analyses were used to assess whether the increases in power within and across conditions were due to phase locking. Separate between-condition analyses were conducted for ERSP, ERP, and ITC measures. Bootstrapped *t*-tests with 1,000 sample sets were applied to the collection of subject-mean projected measures in the two conditions to determine significance between condition differences. For all measures, significance was determined as $P < 0.05$.

High-pain vs. low-pain classification of EEG signals. A custom program was built around MATLAB's machine learning libraries to classify the EEG data into high- and low-pain conditions. Contrasts between ERSP plots of high- and low-pain conditions in the medial prefrontal cortex and contralateral sensorimotor cortex guided feature extraction. Statistically significant regions of ERSP contrast plots were selected to pick the frequency range and time range for extraction of features for classification.

A logistic regression model was fitted to the entire dataset, and the classification accuracy of training was calculated, which provided an upper bound on the classification accuracy that could be obtained from a linear classifier on our dataset. SVM was then used with the linear kernel and then with the Gaussian kernel (radial basis function) via the fitcsvm function of MATLAB. The Gaussian kernel was found to be superior in separating the classes and was therefore used in the final classification. The sequential minimal optimization algorithm was used within the SVM to search for the hyperplane, maximally separating high- and low-pain classes.

The accuracy of the trained classifier was estimated via leave-one-out cross-validation (CV), which was performed by training the classifier on all but one data point and then testing the resulting trained classifier on the left-out data point. This procedure was repeated, such that each data point was used once as the test data point. The accuracy estimates of all of the tests were averaged to obtain one accuracy value, which is called the leave-one-out CV accuracy. For each leave-one-out CV procedure, a grid search was performed on the parameter space of the Gaussian SVM. Combinations of the regularization parameter (C) and the Gaussian kernel parameter (γ), which minimized the leave-one-out CV error, were identified in the grid search procedure.

RESULTS

Pain ratings. Thermal stimuli were delivered to three spatially distinct sites on the right volar forearm to control for habituation and sensitization. Mean temperature for the low-pain condition was 41.75°C (SD = 1.66), and mean temperature for the high-pain condition was 45.37°C (SD = 1.05). To assess pain ratings across time, trials in each block were grouped into a first half and a second half. Pain ratings within each half were then averaged. Then, we performed a three-way ANOVA (condition × block × half) on the pain-rating data. There was no effect of half [$F(1,30) = 0.005$, $P = 0.95$, $\eta^2 < 0.001$] or block [$F(1,30) = 2.87$, $P = 0.10$, $\eta^2 = 0.09$], which confirmed that there were no habituation or sensitization confounds. By design, there was a significant effect of condition [$F(1,30) = 318.4$, $P < 0.001$, $\eta^2 = 0.91$]. The mean pain rating in the high-pain condition was 5.53 (SE = 0.23) and in the low-pain condition was 0.87 (SE = 0.18).

ERSP in the medial prefrontal domain. A total of 14 brain regions, referred to as domains, were found with the MPA and are listed in Table 1. Two criteria were applied to narrow down the selection of domains for further analysis. Domains that had

Table 1. *Domains (brain regions) identified by MPA*

Domain	Subjects	ERSP Contrast	Anatomical Areas	Fraction
1	29	Yes	L Cingulate gyrus	0.19
			R Cingulate gyrus	0.12
			L Superior frontal gyrus	0.19
			L Caudate	0.31
			R Caudate	0.08
2	27	Yes	L Precentral gyrus	0.16
			L Postcentral gyrus	0.23
			L Superior parietal gyrus	0.31
			L Supramarginal gyrus	0.16
			L Precuneus	0.14
3	27	No	R Putamen	0.23
			R Insular cortex	0.21
			R Caudate	0.21
4	27	No	R Inferior frontal gyrus	0.93
5	26	No	R Superior parietal gyrus	0.60
			R Postcentral gyrus	0.17
6	26	No	R Supramarginal gyrus	0.54
			R Postcentral gyrus	0.24
			R Angular gyrus	0.14
7	25	Yes	L Inferior frontal gyrus	0.53
			L Lateral orbitofrontal gyrus	0.34
8	24	Yes	R Postcentral gyrus	0.42
			R Superior parietal gyrus	0.27
			R Precentral gyrus	0.18
9	23	Yes	L Precentral gyrus	0.40
			L Postcentral gyrus	0.29
10	23	Yes	L Superior temporal gyrus	0.34
			L Middle temporal gyrus	0.25
			L Insular cortex	0.12
11	23	No	R Postcentral gyrus	0.64
			R Superior parietal gyrus	0.21
12	18	Yes	Cerebellum	1.00
13	15	No	R Precentral gyrus	0.66
			R Postcentral gyrus	0.34
14	8	No	L Supramarginal gyrus	0.89

For each domain, the following are listed: the number of contributing subjects, whether the ERSP measures of high- and low-pain conditions were significantly different in the domain, the anatomical regions spanned by the domain, and the fraction of the domain in each anatomical region. Anatomical localization of the domain was based on the brain atlas provided by the LONI project. L, left; R, right.

fewer than 90% of the subjects contributing to them and domains that did not show significant differences between conditions in the ERSP plots were excluded from further analysis. Only two domains survived the selection criteria: a domain in the medial prefrontal cortex (domain 1 in Table 1) and a domain in the contralateral sensorimotor cortex (domain 2 in Table 1).

Figure 2*A* shows the medial prefrontal domain, which spanned bilateral cingulate gyrus, bilateral caudate, and the superior frontal gyrus. Figure 2*B* shows the ERSP measure from this domain in the high-pain condition. A strong increase in theta power is evident from 300 to 1,000 ms after heat onset, as shown from 3 to 7 Hz. An increase in gamma power is also evident 500 ms after heat onset, as reflected in the ERSP plot from 50 to 90 Hz. A decrease in power was most prominent in alpha and beta bands, beginning at ~1,000 ms after heat onset. Figure 2*C* shows the ERSP measure from this domain in the low-pain condition. The pattern is similar to that observed in the high-pain condition, but the changes in power are attenuated. Increases in theta power are from 300 to 1,000 ms after heat onset, and mild increases in gamma power are also evident 500 ms after heat onset. A decrease in alpha and beta power is also evident 1,000 ms after heat onset. Figure 2*D* shows statistically significant contrast between the ERSPs of high- and low-pain conditions from the medial prefrontal domain. The strongest contrasts are evident in the theta band and in the gamma band, with the high-pain condition showing a stronger increase in power compared with the low-pain condition. The contrast in the theta band is most pronounced early and may reflect the onset of the stimulus, whereas differences in the gamma band are persistent for the duration of the stimulus and may reflect the steady-state response.

ERSP in the contralateral sensorimotor domain. Figure 2*E* shows the contralateral sensorimotor domain, which spanned contralateral precentral and postcentral gyri, contralateral superior parietal gyrus, and contralateral supramarginal gyrus. Figure 2*F* shows the ERSP measure from this domain in the high-pain condition. A strong decrease in alpha and beta power

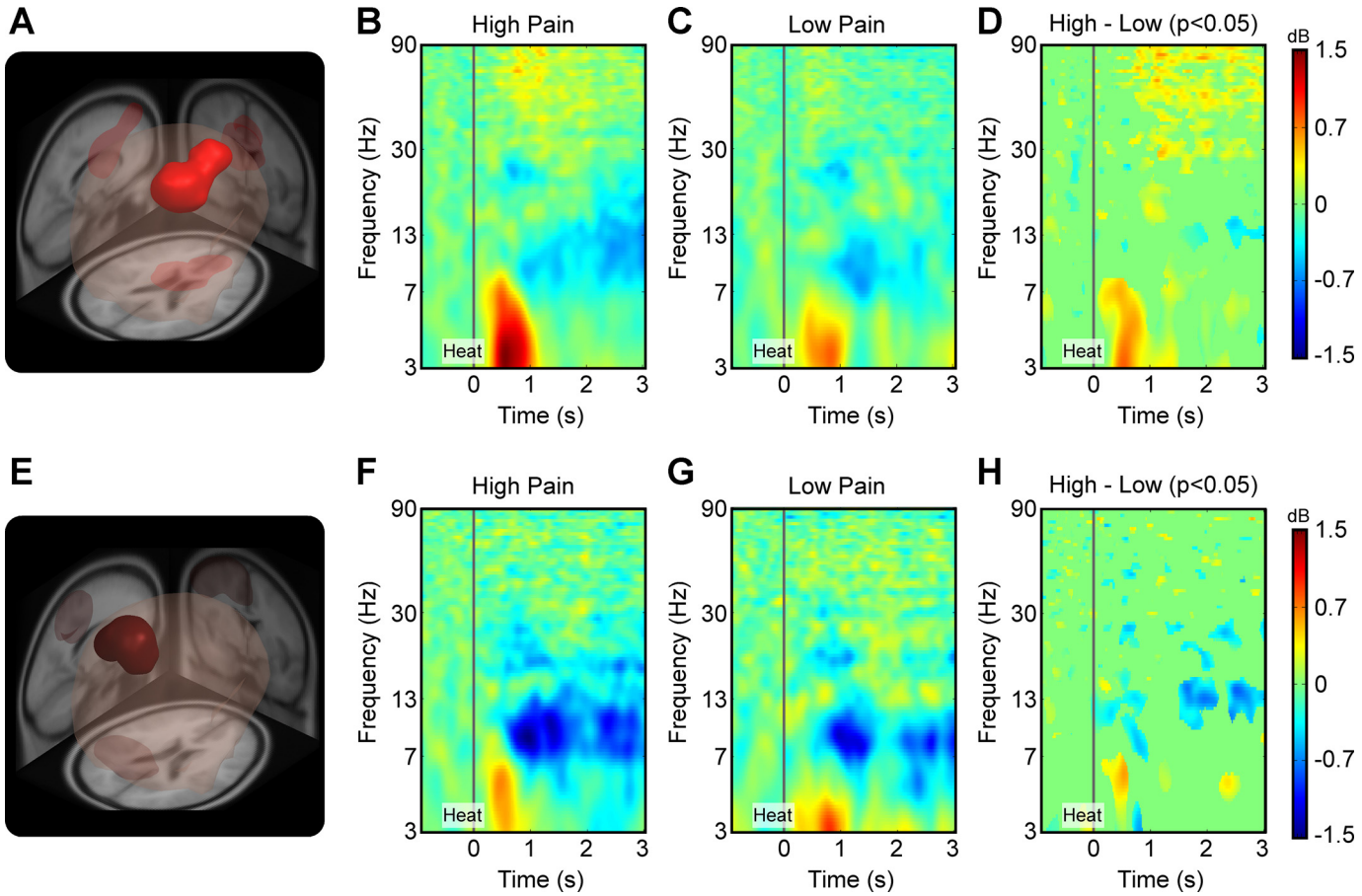

Fig. 2. Measure projection analysis of the event-related spectral perturbation (ERSP) measure yielded significant domains of activity in the brain. *A*: the first significant domain ($P < 0.05$) was found in the medial prefrontal cortex, bilaterally spanning the superior frontal gyrus, the cingulate gyrus, and the caudate. Anatomical localization of the domain was based on the brain atlas provided by the LONI project (Shattuck et al. 2008) and is listed in Table 1. *B*: ERSP measure from the medial prefrontal domain in the high-pain condition. The heat stimulus onset at time = 0 s was treated as the event in all conditions. The 1.5-s time window before the event served as the baseline, relative to which spectral perturbations were calculated over the 4.0-s window after the event. Sinusoidal wavelet transform, which was used to convert the EEG data to time-frequency space, led to truncation of 0.75 s from each end of the ERSP plot. Dark red, heat onset from 3 to 7 Hz; yellow-red, increase in gamma power, 500 ms after heat onset, from 50 to 90 Hz; blue, decrease in power. *C*: ERSP measure from the domain in the low-pain condition. *D*: contrast plot showing statistically significant differences ($P < 0.05$) between the ERSP measure of high- and low-pain conditions from the aforementioned domain. *E*: a significant domain ($P < 0.05$) was found in the contralateral sensorimotor cortex spanning the precentral gyrus, postcentral gyrus, superior parietal gyrus, and supramarginal gyrus. *F*: ERSP measure from the contralateral sensorimotor cortex domain in the high-pain condition. *G*: ERSP measure from the same domain in the low-pain condition. *H*: contrast plot showing statistically significant differences ($P < 0.05$) between the ERSP measure of high- and low-pain conditions.

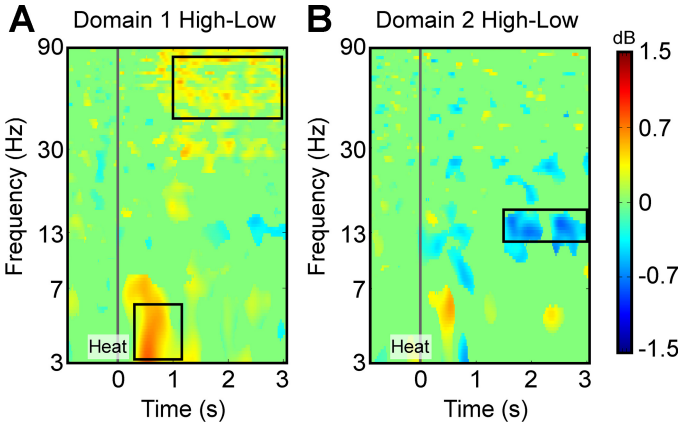

Fig. 3. Selection of feature space for machine learning-based classification of EEG data into high- and low-pain classes. *A*: the ERSP contrast plot from the medial prefrontal domain (Fig. 2*D*). The areas showing the strongest contrast were selected as the regions of interest (ROIs) and are marked by black boxes. *B*: the ERSP contrast plot from the contralateral sensorimotor domain (Fig. 2*H*). The area showing the strongest contrast was selected as the ROI and is marked by the black box. Pixels over each ROI were averaged within each condition and for each individual to yield a feature space comprising ERSP values in gamma, theta, and beta bands.

is evident 500 ms after heat onset and persists for the duration of the stimulation period. A slight increase in theta power is also evident between 300 and 700 ms after heat onset but then quickly dissipates. Figure 2*G* shows the ERSP measure in the low-pain condition. Consistent with the pattern in the high-pain condition, a decrease in alpha and beta power is evident 500 ms after heat onset, and small increases in theta power are evident 100 to 1,100 ms after heat onset. Figure 2*H* shows statistically significant contrast between the ERSPs of high- and low-pain conditions for the contralateral sensorimotor domain. The strongest contrast is evident in the lower beta band, with the high-pain condition showing a significant decrease in power compared with the low-pain condition.

Classification. We used machine learning to classify the EEG data of subjects into high- and low-pain classes. Given that the number of features in a classification procedure should be approximately one-tenth of the number of the data point, and our maximum number of data points per class was 30, we restricted the number of features to 3. The features were selected from the ERSP plots shown in Fig. 2, *B*, *C*, *F*, and *G*. The high-pain vs. low-pain contrasts, shown in Fig. 2, *D* and *H*, were used to guide the selection of ERSP features for classification. As shown in Fig. 3*A*, two regions of interest (ROIs) were identified on the ERSP contrast plot from domain 1, which was the medial prefrontal domain. The first ROI was in the gamma band from 50 to 80 Hz and from 1,000 to 3,000 ms after heat onset. The second ROI was in the theta band from 3 to 6 Hz and from 200 to 1,200 ms after heat onset. Figure 3*B* shows the third ROI, identified on the ERSP contrast plot from domain 2, which was the contralateral sensorimotor domain. This ROI was in the lower beta band from 12 to 16 Hz and from 1,500 to 3,000 ms after heat onset.

The ERSP values were averaged over each of the three ROIs within each condition for each subject. Hence, the 3D feature space included the average ERSP values for the gamma and theta bands in the medial prefrontal domain and the beta band in the contralateral sensorimotor domain. First, we fitted a logistic regression model to the entire dataset and calculated the classification accuracy of training. The classification accuracy of training was 91%. This gave us an upper bound on the classification accuracy that could be obtained from a linear classifier on our dataset.

Next, we used a linear kernel SVM classifier. We performed a search on the C to find the highest leave-one-out CV accuracy possible with linear SVM when including all features. The maximum CV accuracy found was 81.25%. Conversely, Fig. 4*A* shows that the minimum CV error rate was 0.1875 or 18.75%. A Gaussian kernel (radial basis function) SVM classifier was next used to determine whether the classification

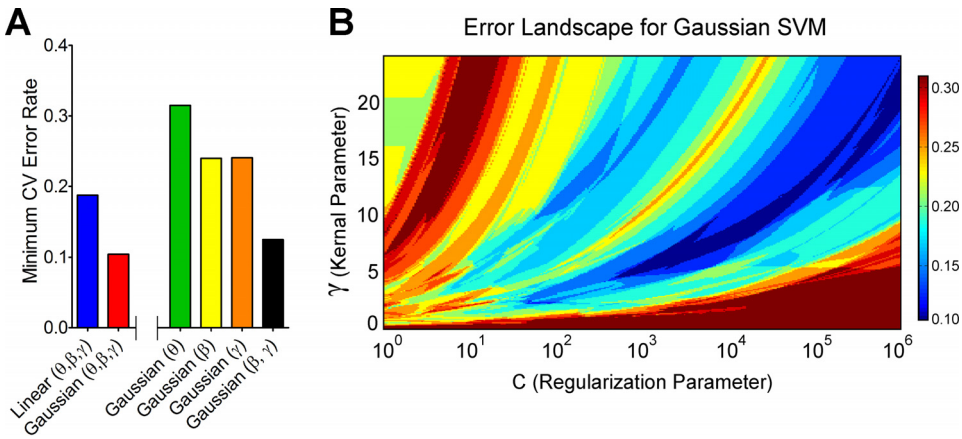

Fig. 4. *A*: the minimum cross-validation (CV) error rate obtained for high/low-pain classification using linear kernel support vector machine (SVM) and Gaussian kernel SVM for different combinations of features. See descriptions of bar colors on *x*-axis. *B*: CV error landscape in the parameter space of Gaussian SVM. The logarithmic *x*-axis is the regularization parameter (C), and the *y*-axis is the Gaussian kernel parameter (γ) of the SVM model. The color scale depicts leave-one-out CV error rate. The dark blue color represents where the minimum CV error rate of 0.1042 was found. This region spans a wide range of values in C (>3 orders of magnitude). The trajectory of the region shows a positive slope, which is an expected pattern in model validation. Since increasing the value of C makes SVM models susceptible to overfitting, and increasing the value of γ makes them susceptible to underfitting, C and γ must increase together to keep the balance. It is impossible to search the entire parameter space. However, we can make inferences about the error landscape in the unexplored regions of the grid based on the patterns seen in the explored regions. The patterns are usually simpler when there are fewer features in the model and hence are informative about the unexplored regions of the parameter space. The pattern shows that the minimum error of 0.1042 or 10.42% is expected to be observed even in the unexplored regions of the parameter space.

accuracy could be improved. We performed a search on the C and the γ to find the highest leave-one-out CV accuracy possible with Gaussian SVM. The maximum CV accuracy found was 89.58%. Conversely, Fig. 4*A* shows that the minimum CV error rate was 0.1042 or 10.42%. Hence, the Gaussian kernel SVM outperformed the linear kernel SVM, implying that a nonlinear decision boundary is more suitable than a linear decision boundary for this classification problem. Figure 4*B* shows the error landscape for Gaussian SVM in the model parameter space, γ vs. C. We demonstrate that the minimum error (0.1042 or 10.42%) is observed in a large region of the explored parameter space, as shown in Fig. 4*B*.

Next, we determined which of the three features contributed the most to the classification accuracy. With the use of only the theta band as a feature and Gaussian SVM as the classifier, we found the leave-one-out CV accuracy to be 68.52% (minimum CV error rate = 0.3148; Fig. 4*A*). With the use of the beta band as the only feature, the accuracy rate was 76% (minimum CV error rate = 0.24; Fig. 4*A*). With the use of the gamma band as the only feature, the accuracy rate was 75.93% (minimum CV error rate = 0.2407; Fig. 4*A*). Hence, gamma and beta bands contributed substantially more than the theta band. Given the large accuracy difference between theta and the remaining bands, we calculated the classification accuracy in the absence of theta by including only gamma and beta bands in the feature space. We found the maximum leave-one-out CV accuracy to be 87.5% (minimum CV error rate = 0.125; Fig. 4*A*), which is close to the 89.58% accuracy obtained by including all three features. This suggests that gamma and beta bands, which represented the steady-state responses to the stimulation, were the more important features when classifying pain states in the current paradigm.

ERPs and ITC. Figure 2, *B* and *C*, shows an increase in theta power in both conditions immediately following heat onset. Previous pain-related studies have also reported increased theta power, which has been attributed to a combination of phase-locked and nonphase-locked oscillations (Bromm and Treede 1991; Iannetti et al. 2005; Ohara et al. 2004). We used ERP and ITC analyses to determine whether the increase in theta power in the medial prefrontal domain could be attributed to phase locking to the onset of the heat stimulus. No statistically significant ERP domain was found to overlap with the medial prefrontal domain from the ERSP analysis. However, we found a statistically significant ($P < 0.05$) ITC domain that partially overlapped with the ERSP domain in the medial prefrontal area. The ITC domain was localized to the cingulate cortex (27%) and the caudate (73%). Evidence for phase locking was found in frequencies up to 6 Hz within 1.5 s of the heat onset. The phase locking was statistically stronger in the high-pain condition compared with the low-pain condition. The ITC analysis demonstrates that phase locking partially contributed to the increase in power in the theta band in the medial prefrontal domain after heat onset.

DISCUSSION

In the current study, we collected high-density EEG data during an experimental paradigm in which subjects experienced a 4-s, low- or high-intensity pain-eliciting stimulus. We implemented a novel, unconstrained whole-brain analysis approach to determine whether frequency-specific cortical oscillations beyond the sensorimotor cortex contribute to the EEG signal of pain perception. We report three novel findings. First, an increase in pain perception was associated with an increase in gamma and theta power in a domain that included the medial prefrontal cortex. Second, a decrease in lower beta power was associated with an increase in pain perception in a domain that included the contralateral sensorimotor cortex. Third, we demonstrate that theta and gamma power in the medial prefrontal cortex and lower beta power in the contralateral sensorimotor cortex can be used to classify EEG signals into high- and low-pain classes with close to 90% accuracy.

Increases in pain perception were associated with an increase in gamma and theta power in a domain that included medial prefrontal cortex. Our observations complement a body of imaging work that has associated pain with the medial prefrontal cortex (Apkarian et al. 2009; Baliki et al. 2012; Jones et al. 1991; Parks et al. 2011; Schulz et al. 2015; Vachon-Presseau et al. 2016). The first EEG experiment to associate pain with gamma oscillations in medial prefrontal cortex did so using an elegant experimental paradigm in which individuals experienced a pain-eliciting stimulus for 10 min (Schulz et al. 2015). Although conventional pain-related EEG studies have used short-duration laser stimuli on the order of 3–5 ms, here, we used a 4-s-long pain-eliciting stimulus. Hence, the first novel finding in the current study is that pain-eliciting stimuli on the order of seconds are sufficient to engage prefrontal gamma oscillations in medial prefrontal cortex. Our observations are consistent with a nonhuman primate study, which showed that functional activity in the medial prefrontal cortex is associated with the perception of somatosensory stimuli (Romo and de Lafuente 2013). Subjective perception is a fundamental component of the pain experience and relies on the integration of sensory, emotional, and cognitive processes. The medial prefrontal cortex has been identified as an important hub that is involved in this functional integration (Etkin et al. 2011; Misra and Coombes 2015; Perini et al. 2013; Shackman et al. 2011) and in assigning behavioral relevance or salience to context (Borsook et al. 2013; Legrain et al. 2011). For instance, uncontrollable compared with controllable pain leads to increased activity in medial prefrontal cortex, even when the intensity of the stimulus is constant across conditions (Brascher et al. 2016).

The medial prefrontal cortex contains a number of anatomically distinct regions, including the anterior cingulate cortex (ACC) and the anterior and posterior midcingulate cortex (MCC) (Vogt 2005). The ACC projects to the amygdala, periaqueductal gray, and the parabrachial nucleus, whereas the MCC projects to the spinal cord and motor cortices. Over the last several decades, neuroimaging, electrophysiological, and anatomical data have converged to support the functional segregation model of cingulate cortex, with ACC associated with affective processing, anterior MCC with cognitive control and fear avoidance, and posterior MCC with skeletomotor function (Bush et al. 2000; Vogt 2005). However, several recent studies have associated anterior MCC with motor function (Dum et al. 2009; Mutschler et al. 2009), pain processing (Peltz et al. 2011; Vogt 2005), cognitive control (Nee et al. 2011), and emotion processing (Kober et al. 2008), leading some to question the segregation model (Shackman et al. 2011). The domain that we identified in the current study overlapped multiple regions, including the bilateral cingulate

gyrus, bilateral caudate, and superior frontal gyrus, which limited our ability to specify generators separately within each of these regions. Nevertheless, the position of our domain demonstrates that the processing of longer-duration pain-eliciting stimuli was not limited to sensory processing in the somatosensory or sensorimotor cortex and extended to medial prefrontal regions. Moreover, the location of our frontal domain was consistent with the anterior MCC more so than regions of the posterior MCC or ACC, consistent with the position that the anterior MCC is an integrative hub within the pain-processing network (Misra and Coombes 2015; Shackman et al. 2011; Wager et al. 2016).

Evidence from animal and human studies points to an association between stimulus intensity and gamma power over sensorimotor regions (Hauck et al. 2015; Ross et al. 2013; Rossiter et al. 2013; Sumiyoshi et al. 2012). The association between gamma power and stimulus intensity over sensorimotor areas has been founded on experimental paradigms that use very short-duration laser stimuli. Hence, although there is much evidence to support the position that sensory processing of short-duration pain-eliciting stimuli may faithfully translate to the subjective perception of pain (Gross et al. 2007; Rossiter et al. 2013; Schulz et al. 2015), longer-duration pain-eliciting stimuli do not appear to scale with gamma oscillations over sensorimotor regions. In the current study, the increase of the intensity of a 4-s pain-eliciting stimulus did not lead to an increase in gamma power in sensorimotor areas. We observed a decrease in lower beta power with an increase in pain perception in a domain that included the contralateral sensorimotor cortex and superior parietal cortex. Our findings are consistent with previous studies that have shown decreases in beta power over somatosensory and sensorimotor areas (Crone et al. 1998; Mancini et al. 2013; Ploner et al. 2006; Rossiter et al. 2013) and previous fMRI studies that have associated activity in the somatosensory and sensorimotor areas with the experience of pain (Gelnar et al. 1999; Misra and Coombes 2015; Wager et al. 2013). Pain-related decreases in beta power over sensorimotor cortex have been interpreted as reflecting both bottom-up and top-down processes. Support for bottom-up processing comes from studies that report negative correlations between beta power and stimulus intensity in sensorimotor cortex (Hauck et al. 2015). Support for top-down processing comes from evidence that shows that pain-related suppression of beta oscillations over contralateral premotor areas leads to shorter reaction times for voluntary movement (Misra et al. 2016), consistent with the idea that beta-band oscillations are anti-kinetic and reflect the current sensorimotor state (Engel and Fries 2010). The current study was designed such that low-pain stimuli and high-pain stimuli corresponded with low-pain perception and high-pain perception for each individual. The delineation of EEG correlates of stimulus intensity from pain intensity, as demonstrated previously (Schulz et al. 2015), was therefore not possible in the current study. Nevertheless, converging evidence from neurophysiological studies in humans and animals suggests that gamma oscillations in medial prefrontal cortex are associated with the subjective perception of a pain-eliciting stimulus that lasts minutes, whereas beta oscillations over sensorimotor areas are associated with stimulus intensity (Schulz et al. 2015). The current observations are consistent with this position and suggest that a pain-eliciting stimulus that lasts for 4 s is sufficient to elicit increases in gamma power in the medial prefrontal cortex.

To classify the EEG signals into high- and low-pain classes, we used theta and gamma power in the medial prefrontal domain and lower beta power in the contralateral sensorimotor domain as the three features and Gaussian SVM as the classifier. We found a leave-one-out CV accuracy of 89.58%. EEG signals have been used before to classify individuals as being low or highly sensitive to pain in a paradigm where the intensity of the pain-eliciting stimulus was held constant across individuals (Schulz et al. 2012). The reported peak classification accuracy reached 83% based on theta power and gamma power extracted from specific frequencies (8 and 80 Hz) and specific electrodes (FC1, FC2, and C2). Our classification accuracy of 89% is similar to the 83% reported by Schultz et al. (2012), but our findings are notably different for five reasons. First, we used a stimulus that was 4 s long compared with a laser stimulus that was 4 ms long. Second, we manipulated stimulus intensity to control for pain perception for each individual, rather than holding the stimulus constant across individuals and classifying based on high or low sensitivity to pain. Third, our analyses were conducted in source space compared with electrode space. Fourth, we extracted data from windows that were quite broad, both in terms of time and frequency. Fifth, our observations suggest that gamma power rather than theta power in medial prefrontal regions contributes most to the classification of pain perception. Differences in theta power were evident early after stimulus onset and then dissipated, as is commonly seen following short-duration laser stimuli (Brodersen et al. 2012; Ploner et al. 2006). In contrast, differences in gamma power for high- and low-pain conditions were evident from 500 ms after stimulus onset and were preserved throughout the stimulation period. When using individual frequency bands as classifiers, we found that the leave-one-out CV accuracy for gamma was 75.93%, and for theta, it is was 68.52%. Accuracy rate was 76% when using the beta band as the only feature. When combining gamma and beta power in the feature space and excluding theta, we found the maximum leave-one-out CV accuracy to be 87.5%, which was close to the 89.58% accuracy obtained by including all three features. Our observations demonstrate that frequency bands that reflect the steady-state response most accurately classify pain perception in the current paradigm. Our findings suggest that stimulus duration is a key feature that should be considered when using EEG signals to classify pain states.

It is well established that chronic pain states cannot be fully attributed to abnormalities in sensory processing and that brain circuits that span sensory, cognitive, and emotional networks likely play an integral role in chronic pain (Apkarian et al. 2009; Baliki et al. 2012; Vachon-Presseau et al. 2016). The majority of previous work using brief laser-evoked stimuli has induced gamma oscillations only in somatosensory and sensorimotor areas. Such approaches may accurately reflect the sensory processes associated with pain. However, short-duration laser stimuli may not be long enough to elicit changes in prefrontal regions that are associated with chronic pain states. Our observations provide new evidence to support the position that stimulus duration is a key factor that will alter which spatial locations and frequency bands encode pain (Schulz et al. 2015). Here, we show that a 4-s pain-eliciting stimulus is sufficient to elicit increases in gamma power in prefrontal

regions. However, it is important to note that we used 48 trials per condition to identify the domains, and features were extracted from each individual's average ERSP plot across all 48 trials in each condition. The current approach may therefore not be optimal for classifying pain states based on individual trials. Future studies will also be necessary to determine the minimum stimulus duration that is needed to replicate our findings.

The development of paradigms and analyses that elicit, evaluate, and combine pain-related gamma responses in medial prefrontal areas with beta responses in sensorimotor areas is an important step forward. Our classification analysis was based on data from multiple brain regions and multiple frequency bands and distinguished high pain from low pain. Accurate classification of chronic pain states will likely be derived from measures that vary in amplitude across multiple brain regions, given the multidimensional nature of chronic pain (Lopez-Sola et al. 2017; Wager et al. 2013). Previous pain classification studies have used functional neuroimaging data from multiple brain regions to discriminate painful heat from nonpainful warmth with ~95% accuracy and physical pain from social pain in healthy adults with 76% accuracy (Wager et al. 2013). Other classification experiments have used EEG signals from individual electrodes to classify healthy individuals as, more or less, sensitive to pain with 83% accuracy (Schulz et al. 2012), and structural MRI studies have used gray matter intensity measures across multiple regions to classify individuals with chronic pelvic pain and healthy controls with 73% accuracy (Bagarinao et al. 2014). The current study adds to this literature by discriminating low-pain states from high-pain states in healthy adults. Such an approach may be useful to understand the neurophysiological mechanisms that underlie interventions for pain relief (Hu et al. 2015; Li 2013; Li et al. 2013, 2014; Misra et al. 2014; Paris et al. 2013), especially when interventions lower pain without abolishing it.

GRANTS

Grant support for S. A. Coombes was provided by the National Institute of Neurological Disorders and Stroke, Florida Biomedical Research Foundation, and American Heart Association.

DISCLOSURES

S. A. Coombes is cofounder and manager of Neuroimaging Solutions, Gainesville, FL.

AUTHOR CONTRIBUTIONS

G.M. and S.A.C. performed experiments; G.M. and S.A.C. analyzed data; G.M. and S.A.C. interpreted results of experiments; G.M. and S.A.C. prepared figures; G.M. and S.A.C. drafted manuscript; G.M., W.-e.W., D.B.A., A.R., and S.A.C. edited and revised manuscript; G.M., W.-e.W., D.B.A., A.R., and S.A.C. approved final version of manuscript.

REFERENCES

Amari S, Cichocki A, Yang HH. A new learning algorithm for blind signal separation. *Adv Neural Inf Process Syst* 757–763, 1996.

Apkarian AV, Baliki MN, Geha PY. Towards a theory of chronic pain. *Prog Neurobiol* 87: 81–97, 2009.

Bagarinao E, Johnson KA, Martucci KT, Ichesco E, Farmer MA, Labus J, Ness TJ, Harris R, Deutsch G, Apkarian AV, Mayer EA, Clauw DJ, Mackey S. Preliminary structural MRI based brain classification of chronic pelvic pain: a MAPP network study. *Pain* 155: 2502–2509, 2014.

Baliki MN, Petre B, Torbey S, Herrmann KM, Huang L, Schnitzer TJ, Fields HL, Apkarian AV. Corticostriatal functional connectivity predicts transition to chronic back pain. *Nat Neurosci* 15: 1117–1119, 2012.

Beck AT, Steer RA. *BDI, Beck Depression Inventory: Manual*. San Antonio, TX: Psychological Corp, 1987.

Bell AJ, Sejnowski TJ. An information-maximization approach to blind separation and blind deconvolution. *Neural Comput* 7: 1129–1159, 1995.

Benjamini Y, Hochberg Y. Controlling the false discovery rate: a practical and powerful approach to multiple testing. *J R Stat Soc Series B Stat Methodol* 57: 289–300, 1995.

Bigdely-Shamlo N, Mullen T, Kreutz-Delgado K, Makeig S. Measure projection analysis: a probabilistic approach to EEG source comparison and multi-subject inference. *Neuroimage* 72: 287–303, 2013.

Borsook D, Edwards R, Elman I, Becerra L, Levine J. Pain and analgesia: the value of salience circuits. *Prog Neurobiol* 104: 93–105, 2013.

Borsook D, Moulton EA, Schmidt KF, Becerra LR. Neuroimaging revolutionizes therapeutic approaches to chronic pain. *Mol Pain* 3: 25, 2007.

Brascher AK, Becker S, Hoeppli ME, Schweinhardt P. Different brain circuitries mediating controllable and uncontrollable pain. *J Neurosci* 36: 5013–5025, 2016.

Brodersen KH, Wiech K, Lomakina EI, Lin CS, Buhmann JM, Bingel U, Ploner M, Stephan KE, Tracey I. Decoding the perception of pain from fMRI using multivariate pattern analysis. *Neuroimage* 63: 1162–1170, 2012.

Bromm B, Treede RD. Laser-evoked cerebral potentials in the assessment of cutaneous pain sensitivity in normal subjects and patients. *Rev Neurol (Paris)* 147: 625–643, 1991.

Bush G, Luu P, Posner MI. Cognitive and emotional influences in anterior cingulate cortex. *Trends Cogn Sci* 4: 215–222, 2000.

Coghill RC, Sang CN, Maisog JM, Iadarola MJ. Pain intensity processing within the human brain: a bilateral, distributed mechanism. *J Neurophysiol* 82: 1934–1943, 1999.

Coombes SA, Misra G. Pain and motor processing in the human cerebellum. *Pain* 157: 117–127, 2016.

Crone NE, Miglioretti DL, Gordon B, Sieracki JM, Wilson MT, Uematsu S, Lesser RP. Functional mapping of human sensorimotor cortex with electrocorticographic spectral analysis. I. Alpha and beta event-related desynchronization. *Brain* 121: 2271–2299, 1998.

Delorme A, Makeig S. EEGLAB: an open source toolbox for analysis of single-trial EEG dynamics including independent component analysis. *J Neurosci Methods* 134: 9–21, 2004.

Dum RP, Levinthal DJ, Strick PL. The spinothalamic system targets motor and sensory areas in the cerebral cortex of monkeys. *J Neurosci* 29: 14223–14235, 2009.

Engel AK, Fries P. Beta-band oscillations–signalling the status quo? *Curr Opin Neurobiol* 20: 156–165, 2010.

Etkin A, Egner T, Kalisch R. Emotional processing in anterior cingulate and medial prefrontal cortex. *Trends Cogn Sci* 15: 85–93, 2011.

Gelnar PA, Krauss BR, Sheehe PR, Szeverenyi NM, Apkarian AV. A comparative fMRI study of cortical representations for thermal painful, vibrotactile, and motor performance tasks. *Neuroimage* 10: 460–482, 1999.

Gross J, Schnitzler A, Timmermann L, Ploner M. Gamma oscillations in human primary somatosensory cortex reflect pain perception. *PLoS Biol* 5: e133, 2007.

Hauck M, Domnick C, Lorenz J, Gerloff C, Engel AK. Top-down and bottom-up modulation of pain-induced oscillations. *Front Hum Neurosci* 9: 375, 2015.

Hu H, Li S, Li S. Pain modulation effect of breathing-controlled electrical stimulation (BreEStim) is not likely to be mediated by deep and fast voluntary breathing. *Sci Rep* 5: 14228, 2015.

Iannetti GD, Zambreanu L, Cruccu G, Tracey I. Operculoinsular cortex encodes pain intensity at the earliest stages of cortical processing as indicated by amplitude of laser-evoked potentials in humans. *Neuroscience* 131: 199–208, 2005.

International Association for the Study of Pain. *IASP Taxonomy* (Online). http://www.iasp-pain.org/Education/Content.aspx?ItemNumber=1698&navItemNumber=576 [Oct. 2016].

Jasper HH. Report of the committee on methods of clinical examination in electroencephalography: 1957. *Electroencephalogr Clin Neurophysiol* 10: 370–375, 1958.

Jones AK, Qi LY, Fujirawa T, Luthra SK, Ashburner J, Bloomfield P, Cunningham VJ, Itoh M, Fukuda H, Jones T. In vivo distribution of opioid receptors in man in relation to the cortical projections of the medial and lateral pain systems measured with positron emission tomography. *Neurosci Lett* 126: 25–28, 1991.

Kavanagh RN, Darcey TM, Lehmann D, Fender DH. Evaluation of methods for three-dimensional localization of electrical sources in the human brain. *IEEE Trans Biomed Eng* 25: 421–429, 1978.

Kober H, Barrett LF, Joseph J, Bliss-Moreau E, Lindquist K, Wager TD. Functional grouping and cortical-subcortical interactions in emotion: a meta-analysis of neuroimaging studies. *Neuroimage* 42: 998–1031, 2008.

Kori SH, Miller RP, Todd DD. Kinesiophobia: a new view of chronic pain behavior. *Pain Manag* 3: 35–43, 1990.

Legrain V, Iannetti GD, Plaghki L, Mouraux A. The pain matrix reloaded: a salience detection system for the body. *Prog Neurobiol* 93: 111–124, 2011.

Li S. Breathing-controlled electrical stimulation (BreEStim) for management of neuropathic pain and spasticity. *J Vis Exp* 71: e50077, 2013.

Li S, Berliner JC, Melton DH, Li S. Modification of electrical pain threshold by voluntary breathing-controlled electrical stimulation (BreEStim) in healthy subjects. *PLoS One* 8: e70282, 2013.

Li S, Hu T, Beran MA, Li S. Habituation to experimentally induced electrical pain during voluntary-breathing controlled electrical stimulation (BreEStim). *PLoS One* 9: e104729, 2014.

Lopez-Sola M, Woo CW, Pujol J, Deus J, Harrison BJ, Monfort J, Wager TD. Towards a neurophysiological signature for fibromyalgia. *Pain* 158: 34–47, 2017.

Mancini F, Longo MR, Canzoneri E, Vallar G, Haggard P. Changes in cortical oscillations linked to multisensory modulation of nociception. *Eur J Neurosci* 37: 768–776, 2013.

Misra G, Coombes SA. Neuroimaging evidence of motor control and pain processing in the human midcingulate cortex. *Cereb Cortex* 25: 1906–1919, 2015.

Misra G, Ofori E, Chung JW, Coombes SA. Pain-related suppression of beta oscillations facilitates voluntary movement. *Cereb Cortex*. First published March 10, 2016; doi: 10.1093/cercor/bhw061.

Misra G, Paris TA, Archer DB, Coombes SA. Dose-response effect of isometric force production on the perception of pain. *PLoS One* 9: e88105, 2014.

Mutschler I, Wieckhorst B, Kowalevski S, Derix J, Wentlandt J, Schulze-Bonhage A, Ball T. Functional organization of the human anterior insular cortex. *Neurosci Lett* 457: 66–70, 2009.

Nee DE, Kastner S, Brown JW. Functional heterogeneity of conflict, error, task-switching, and unexpectedness effects within medial prefrontal cortex. *Neuroimage* 54: 528–540, 2011.

Ofori E, Coombes SA, Vaillancourt DE. 3D vortical electrophysiology of ballistic upper limb movement in humans. *Neuroimage* 115: 30–41, 2015.

Ohara S, Crone NE, Weiss N, Treede RD, Lenz FA. Amplitudes of laser evoked potential recorded from primary somatosensory, parasylvian and medial frontal cortex are graded with stimulus intensity. *Pain* 110: 318–328, 2004.

Oshiro Y, Quevedo AS, McHaffie JG, Kraft RA, Coghill RC. Brain mechanisms supporting discrimination of sensory features of pain: a new model. *J Neurosci* 29: 14924–14931, 2009.

Paris TA, Misra G, Archer DB, Coombes SA. Effects of a force production task and a working memory task on pain perception. *J Pain* 14: 1492–1501, 2013.

Parks EL, Geha PY, Baliki MN, Katz J, Schnitzer TJ, Apkarian AV. Brain activity for chronic knee osteoarthritis: dissociating evoked pain from spontaneous pain. *Eur J Pain* 15: 843.e1–814, 2011.

Peltz E, Seifert F, DeCol R, Dorfler A, Schwab S, Maihofner C. Functional connectivity of the human insular cortex during noxious and innocuous thermal stimulation. *Neuroimage* 54: 1324–1335, 2011.

Perini I, Bergstrand S, Morrison I. Where pain meets action in the human brain. *J Neurosci* 33: 15930–15939, 2013.

Ploner M, Gross J, Timmermann L, Pollok B, Schnitzler A. Pain suppresses spontaneous brain rhythms. *Cereb Cortex* 16: 537–540, 2006.

Rhudy JL, Meagher MW. Fear and anxiety: divergent effects on human pain thresholds. *Pain* 84: 65–75, 2000.

Romo R, de Lafuente V. Conversion of sensory signals into perceptual decisions. *Prog Neurobiol* 103: 41–75, 2013.

Ross B, Jamali S, Miyazaki T, Fujioka T. Synchronization of beta and gamma oscillations in the somatosensory evoked neuromagnetic steady-state response. *Exp Neurol* 245: 40–51, 2013.

Rossiter HE, Worthen SF, Witton C, Hall SD, Furlong PL. Gamma oscillatory amplitude encodes stimulus intensity in primary somatosensory cortex. *Front Hum Neurosci* 7: 362, 2013.

Scherg M. Fundamentals of dipole source potential analysis. In: *Auditory Evoked Magnetic Fields and Electric Potentials*, edited by Grandori F, Hoke M, and Romani GL. Basel: Karger, 1990, p. 40–69.

Schulz E, May ES, Postorino M, Tiemann L, Nickel MM, Witkovsky V, Schmidt P, Gross J, Ploner M. Prefrontal gamma oscillations encode tonic pain in humans. *Cereb Cortex* 25: 4407–4414, 2015.

Schulz E, Zherdin A, Tiemann L, Plant C, Ploner M. Decoding an individual's sensitivity to pain from the multivariate analysis of EEG data. *Cereb Cortex* 22: 1118–1123, 2012.

Shackman AJ, Salomons TV, Slagter HA, Fox AS, Winter JJ, Davidson RJ. The integration of negative affect, pain and cognitive control in the cingulate cortex. *Nat Rev Neurosci* 12: 154–167, 2011.

Shattuck DW, Mirza M, Adisetiyo V, Hojatkashani C, Salamon G, Narr KL, Poldrack RA, Bilder RM, Toga AW. Construction of a 3D probabilistic atlas of human cortical structures. *Neuroimage* 39: 1064–1080, 2008.

Spielberger CD. *Manual for the State-Trait Anxiety Inventory (STAI)*. Palo Alto, CA: Consulting Psychologists, 1983.

Sumiyoshi A, Suzuki H, Ogawa T, Riera JJ, Shimokawa H, Kawashima R. Coupling between gamma oscillation and fMRI signal in the rat somatosensory cortex: its dependence on systemic physiological parameters. *Neuroimage* 60: 738–746, 2012.

Tallon-Baudry C, Bertrand O, Delpuech C, Pernier J. Stimulus specificity of phase-locked and non-phase-locked 40 Hz visual responses in human. *J Neurosci* 16: 4240–4249, 1996.

Thomas JS, France CR, Lavender SA, Johnson MR. Effects of fear of movement on spine velocity and acceleration after recovery from low back pain. *Spine (Phila Pa 1976)* 33: 564–570, 2008.

Vachon-Presseau E, Tetreault P, Petre B, Huang L, Berger SE, Torbey S, Baria AT, Mansour AR, Hashmi JA, Griffith JW, Comasco E, Schnitzer TJ, Baliki MN, Apkarian AV. Corticolimbic anatomical characteristics predetermine risk for chronic pain. *Brain* 139: 1958–1970, 2016.

Vogt BA. Pain and emotion interactions in subregions of the cingulate gyrus. *Nat Rev Neurosci* 6: 533–544, 2005.

Wager TD, Atlas LY, Botvinick MM, Chang LJ, Coghill RC, Davis KD, Iannetti GD, Poldrack RA, Shackman AJ, Yarkoni T. Pain in the ACC? *Proc Natl Acad Sci USA* 113: E2474–E2475, 2016.

Wager TD, Atlas LY, Lindquist MA, Roy M, Woo CW, Kross E. An fMRI-based neurologic signature of physical pain. *N Engl J Med* 368: 1388–1397, 2013.

Weiss T, Giersch DA, Sauer H, Miltner WH, Bar KJ. Perception to laser heat stimuli in depressed patients is reduced to Aδ- and selective C-fiber stimulation. *Neurosci Lett* 498: 89–92, 2011.

Winkler I, Haufe S, Tangermann M. Automatic classification of artifactual ICA-components for artifact removal in EEG signals. *Behav Brain Funct* 7: 30, 2011.